Modeling of charge transport in polymers with embedded crystallites

Ya. V. Burdakov,[1] A. Yu. Saunina,[1] H. Bässler,[3] A. Köhler,[2,3] and V. R. Nikitenko[1,*]

[1]*National Research Nuclear University, "MEPhI" (Moscow Engineering Physics Institute), Kashirskoe Shosse 31, 115409 Moscow, Russia*

[2]*Soft Matter Optoelectronics and Bavarian Polymer Institute (BPS), Universitätsstr. 30, D 95448 Bayreuth, Germany*

[3]*Bayreuth Institute of Macromolecular Research (BIMF), Universitätsstr. 30, D 95448 Bayreuth, Germany*

(Received 10 March 2023; accepted 6 July 2023; published 2 August 2023)

Modern organic semiconductors frequently adopt a semicrystalline morphology which makes the analysis of charge transport challenging. In this paper, we employ Monte Carlo (MC) simulation to study the charge-carrier mobility in an amorphous layer—typically 100 nm thick—that contains well-ordered nanosized domains (crystallites). The case of a low carrier concentration, typical for applications in photovoltaics and LEDs, is considered. We study the dependence of mobility on temperature, on the amount (V) of the crystallites, on the energy offset between crystalline and amorphous regions (E_t), and we compare the results with those for a system with solitary traps. We find that, in a system with solitary traps, the mobility can exceed that of the neat phase if the trap depth is comparable with the standard deviation of the density of states (DOS) of the amorphous phase. Controlled by the electronic overlap in the amorphous phase and the crystallites, the mobility in a system with crystallites can increase by up to two orders of magnitude upon increasing V. It features a pronounced maximum when E_t is close to the standard deviation of the DOS of the amorphous phase, while for large values of E_t, the mobility is practically independent of E_t. The results can be rationalized in terms of an interplay between percolation at large E_t and hopping transport within the cumulative densities near the transport of the system. We developed a generalized analytic multiple-trapping-release model to rationalize the results of the MC simulations.

DOI: 10.1103/PhysRevB.108.085301

I. INTRODUCTION

The current development of electronic devices such as LEDs, solar cells, and field-effect transistors with organic semiconductors as active elements has an important impact on basic research. Charge transport, characterized by the charge-carrier mobility, is one of the key physical processes behind the operation of such devices. It is controlled by the semiconductor film morphology and its inherent disorder. Depending on the material and the processing conditions chosen, the active layer, typically a 100-nm-thin film, may contain amorphous, polycrystalline, or crystalline domains. Despite the technological relevance of such systems and a number of experimental and theoretical studies [1–8], there is no comprehensive theoretical description available for the complex morphology-mobility relationship, and an analytical formalism is missing.

The current information on the mechanism by which organic semiconductor morphology affects the charge-carrier mobility is controversial. It is known that, in semicrystalline semiconducting polymers such as poly(3-hexylthiophene) (P3HT), the formation of crystallites increases the hole mobility. The reason is improved structural ordering and an increased wave function overlap due to more dense packing of molecules in a crystalline (aggregated) phase than those in an amorphous phase. This has been concluded from organic field-effect transistor measurements when using P3HTs with increasing molecular weights, which increases the tendency of the P3HT to aggregate [1–3]. On the other hand, grain boundaries in polycrystalline materials inhibit charge transport [4,5]. They can act either as traps or barriers, depending on the position of their mean energy relative to that of the crystalline domains [6,7]. For π-conjugated low-molecular-weight compounds such as perylenebisimides, increased crystallinity in a film has been reported to reduce charge-carrier mobility compared with the amorphous film, whereas a liquid crystalline structure improves it [8].

This paper is a theoretical study of the charge mobility in amorphous films that contain crystallites embedded in an amorphous matrix. It is based upon a combination of Monte Carlo (MC) simulation and analytical theory. In related work, charge transport in organic field-effect transistors has been treated in which the semiconductor is an array of crystallites separated by relatively thin grain boundaries and charge transport is confined to a thin layer. In that case, the concentration of charge carriers is controlled by the gate voltage, and the density of states (DOS) distribution is therefore partially filled [6,9]. In this paper, we consider the alternative case of transport in a thin layer of a semiconductor in which conductive crystallites are embedded in an amorphous phase, but the DOS distribution is only weakly filled. We find that the inclusion of crystallites can enhance charge transport substantially. Under certain conditions, this is even the case when crystallites are replaced by isolated trap sites. Conceptually, for such isolated trap states, charge transport can be described by a multiple

*vladronik@yandex.ru

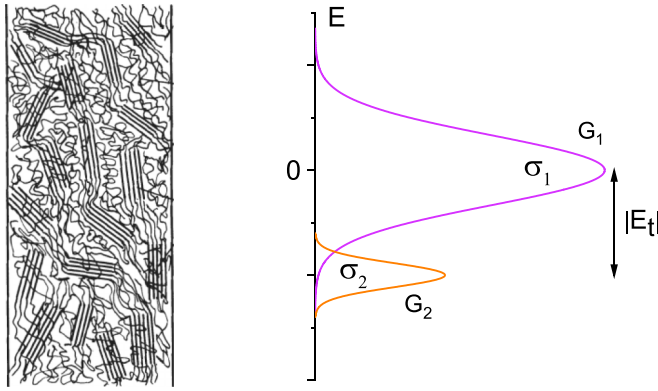

FIG. 1. Schematic view of (a) a polymer layer with amorphous and aggregated regions and (b) the energetic distribution of electronic states in this polymer.

trapping and release (MTR) model in which the effective transport energy E_C is considered a variable. At large energy offset between the amorphous phase and the crystallites, charge transport becomes percolative.

II. THE THEORETICAL MODEL

In a disordered polymer, macromolecules can be arranged in a rather chaotic manner (these regions will be referred to as the amorphous phase), or they can be oriented in a parallel fashion and form aggregated nanoscale regions with reduced disorder. They will be referred to below as the crystallites, see Fig. 1(a).

The energy distribution of localized states in a two-phase material is illustrated in Fig. 1(b). The upper and lower Gaussians of the DOS distribution with the standard deviations σ_1 and $\sigma_2 < \sigma_1$ are related to states from amorphous (G1) and crystallite (G2) phases, respectively. The finite standard deviation σ_2 is due to the imperfect structure of the crystallites, the interaction of an electron inside the crystallite with a disordered (amorphous) neighborhood, and variations of the neighborhood across the sample. The energetic shift of the lower Gaussian E_t is caused by a more compact structure of crystallites and, hence, an increased polarization energy, relative to the amorphous phase. In this paper, we focus on the case that $\sigma_2 = \sigma_1/3$ and $|E_t|$ ranging from $1\sigma_1$ to $8\sigma_1$. The model of the amorphous film with embedded crystallites will be referred to as the M_1 model. The term M_0 model will be used for our reference case, where the extended crystallites are replaced by singular trapping sites. The latter may be a polymer or monomer, depending on whether the amorphous film consists of polymers or monomers. This M_1/M_0 terminology relates to the methodology used in the MC simulations to generate the film morphology.

A. An analytic model based on the MTR concept

In our endeavor to develop a description of charge transport in a M_1 model, we start from the situation where the amorphous film contains merely trapping sites, i.e., the M_0 model. An analytic model for this case has already been developed in Ref. [10]. It rests on both the Gaussian disorder model [11] and the effective transport level concept [12] and leads to a relatively simple formalism of the MTR model [13] to describe hopping transport. The effective transport level E_C is a formal analog of the mobility edge of MTR. One can express the mean release rate from a rather deep state $\omega(E)$ in the same form as in the MTR formalism [12,14]:

$$\omega(E) = \omega_0 \exp\left(-\frac{E_C - E}{kT}\right), \quad E < E_C. \tag{1}$$

In Ref. [10], the transport-level-based MTR formalism was applied to analyze the dependence of mobility on temperature and concentration of G2 states. Note that the case of small concentrations (volume fraction $V \leqslant 1\%$) was considered. As detailed in the Results section below, the comparison between analytic and MC results in this paper shows that this simple transport-level concept is not sufficiently accurate for the case of rather large values of V. For this reason, we apply here the recently developed generalized version of the hopping MTR formalism [15,16]. One can use the MTR formalism if one knows which charge carriers are mobile, i.e., occupy conducting states, and which are immobile, i.e., trapped, irrespective to the form of the $\omega(E)$ dependence. We identify a *conductive* state by the condition that the escape time from this state does not exceed a certain time t_0 [17]. Further, according to the MTR formalism, we define the mobility as

$$\mu = \mu_f \frac{p_f}{p} = \mu_f \frac{\int_{-\infty}^{\infty} dE\, g_{\rm occ}(E)\varphi(E)}{\int_{-\infty}^{\infty} dE\, g_{\rm occ}(E)}, \tag{2}$$

where $\mu_f \approx (e/kT)(a^2/t_0)$ is the mobility of charge carriers in conductive states, a is the lattice constant, p_f and p are the concentrations of mobile carriers and the total concentration, respectively, $\varphi(E)$ is the probability that a given state is conductive, and $g_{\rm occ}(E)$ is the distribution of occupied states (also known as ODOS), which is proportional to the product $g(E)\exp(-E/kT)$, provided quasiequilibrium is established and the concentration of charge carriers is small. Using the Poisson distribution, $\varphi(E) = 1 - \exp[-\omega(E)t_0] \approx \omega(E)t_0$, provided that the critical time t_0 is rather small relative to a typical hopping time in the relevant energy range. Thus, the parameter t_0 cancels in Eq. (2), and the mobility becomes proportional to the mean release rate $\omega(E)$ averaged over the distribution of occupied states. The mean release rate is calculated in a more general way than from the transport level concept. Formally, it implies that, in Eq. (1), E_C is not a constant but a function of energy, see Sec. IV about calculations of the function $E_C(E)$. From Eqs. (1) and (2), one obtains

$$\mu \approx \frac{e\omega_0 a^2}{kT} \frac{\int_{-\infty}^{\infty} dE\, g(E) \exp\left[-\frac{E_C(E)}{kT}\right]}{\int_{-\infty}^{\infty} dE\, g(E) \exp\left(-\frac{E}{kT}\right)}. \tag{3}$$

B. Developing a grid model for the morphology of the material

To allow for MC simulations of the charge transport, a grid model for the film morphology is required. Operationally, the modeled material is constructed from pointlike

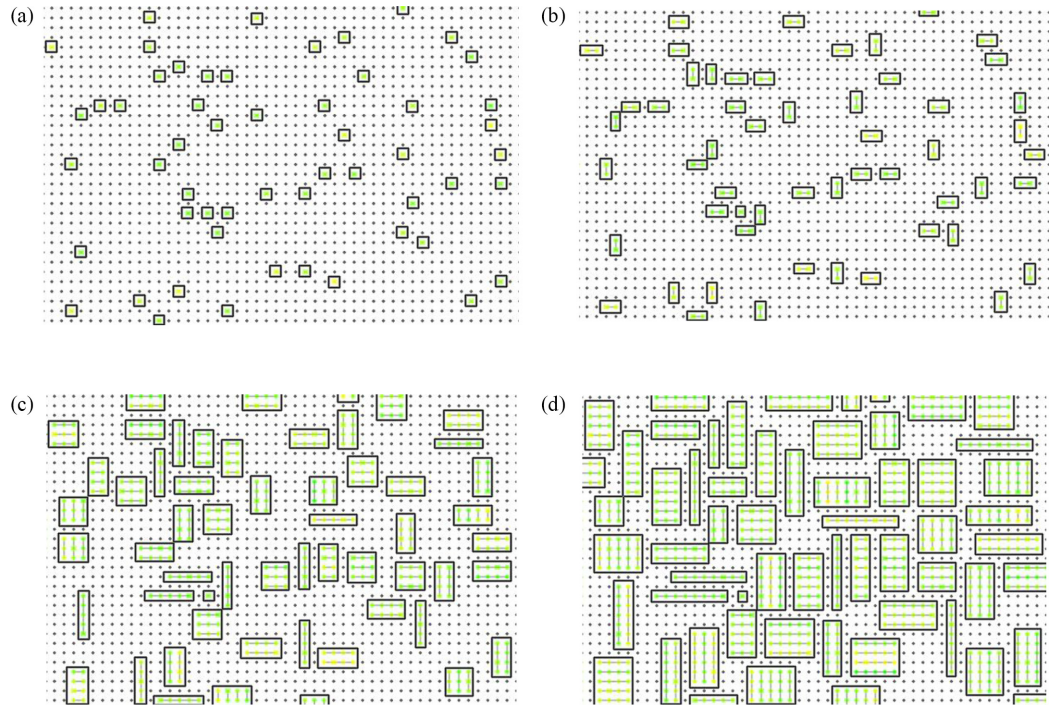

FIG. 2. Illustration of how a two-phase structure is generated. (a) Generating of the points where the crystallites grow. (b) Defining the orientations of chains in the crystallites. (c) The structure after 5 cycles of growth. (d) The final structure.

localized states (hopping sites), representing either small organic molecules or segments of a polymer chain. These sites form a simple cubic lattice, and they are randomly distributed in energy. Some fraction of the sites V belongs to a set of rectangular boxes, i.e., the crystallites, which are randomly centered and randomly distributed in their volumes. The energies of this fraction of sites are randomly distributed according to the lower Gaussian distribution, see Fig. 1(b). This set of boxes forms a crystalline phase. Each box is surrounded by the pointlike localized states, which form an amorphous phase, see Fig. 2(d).

With the developed algorithm of the generation of this random two-phase structure, we are trying to mimic growth of the crystallites in the amorphous phase. Figure 2 is a two-dimensional illustration of this procedure. In the first step, the randomly distributed nucleation centers for subsequent crystallite growth are chosen as illustrated in Fig. 2(a). Their relative concentration is n. In the second step, at every crystallite, another site is attached in a randomly given direction, see Fig. 2(b). Subsequently, every crystallite grows by attachment of either a site in a given direction or a parallel neighbor chain of an achieved length, see Fig. 2(c). The growth of a given crystallite is stopped if the next step necessarily leads to the contact with another crystallite or after having executed a maximal number of steps M. An example of a final structure is shown in Fig. 2(d).

The model has only two intrinsic parameters, i.e., the relative concentration of grow points n and the maximal number of the grow steps M. However, it is more convenient to work with other physically more objective parameters, namely, the relative volume of a crystallite phase V and the mean size of crystallites $\langle l \rangle$. Table S1 in the Supplemental Material [18] shows how the intrinsic and objective parameters are related.

As illustrated in Fig. 1(b), the energy distribution of states (i.e., the sites of cubic lattice) is defined as

$$g(E) = a^{-3}\left\{\frac{(1-V)}{\sqrt{2\pi\sigma_1^2}}\exp\left(-\frac{E^2}{2\sigma_1^2}\right) + \frac{V}{\sqrt{2\pi\sigma_2^2}}\exp\left[-\frac{(E-E_t)^2}{2\sigma_2^2}\right]\right\}. \quad (4)$$

The states belonging to the upper and lower Gaussians are referred to below as the G1 and G2 states, respectively.

C. MC modeling of the charge transport

An electron generated in the middle of the left boundary plain of the layer performs a field-assisted random hopping motion until the right boundary plain is reached. The electric field is applied perpendicular to the boundaries. Hopping rates between localized states are described by the Miller-Abrahams model:

$$\nu(E, E', r) = \nu_0 \exp\left[-2\gamma r - \frac{(E'-E)+|E'-E|}{2kT}\right], \quad (5)$$

where r is the hopping distance, E and E' are the energies of initial and final states, γ is the inverse localization radius of the wave function of the electron, ν_0 is the frequency factor, T is the temperature, and k is the Boltzmann constant, respectively.

For the M_1 model, we consider that the crystallites are formed by localized states, but the transitions of the carrier involving G2 states occur faster than the G1 → G1

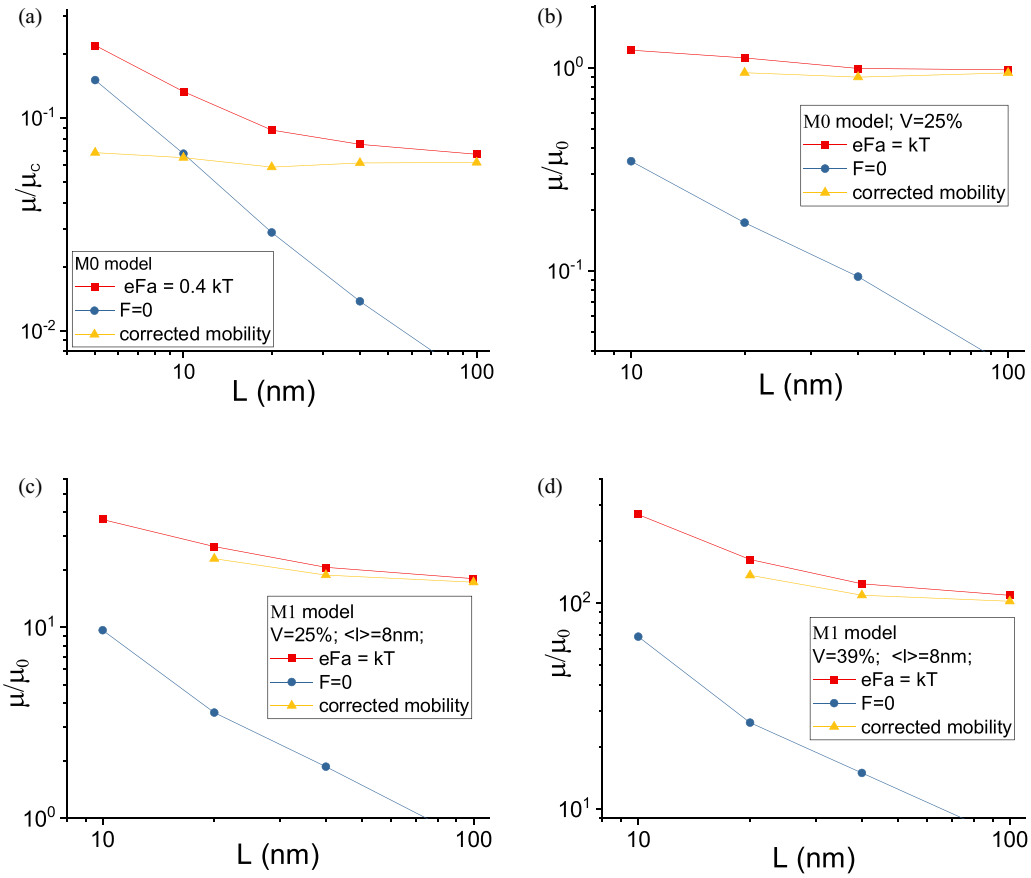

FIG. 3. Illustration of the contribution of diffusion to the mobility as defined from Eq. (7) in an amorphous material with (a) $V = 0$ and (b) $V = 0.25$; in a two-phase material with (c) $V = 0.25$ and (d) $V = 0.39$. $T = 298$ K, $\sigma_1 = 50$ meV, $\sigma_2 = \sigma_1/3$, $E_t = -2\sigma_1$, $2\gamma_2 a = 5$, and $2\gamma_1 a = 10$; $\mu_C = (e/kT)\nu_0 a^2 \exp(-2\gamma a)$, μ_0 is the mobility value at $V = 0$.

transitions because of the reduced disorder in crystallites and the reduced localization parameter of the G2 states. To reflect the faster transition rate within, from, and to the crystallites, we assume $2\gamma_2 a = 5$ for G2 → G2, G2 → G1, and G1 → G2 transitions, while $2\gamma_1 a = 10$ for G1 → G1 transitions. We also consider a maximum hopping distance $r_{\max} = 2.5a$.

For the sake of comparison, calculations were also performed for the M_0 model, i.e., for the case of an amorphous material with singular traps. Both G1 and G2 states are associated with a common coupling parameter of $2\gamma a = 10$ with $\gamma = \gamma_1 = \gamma_2$. The G2 states are randomly distributed in the nodes of the cubic lattice. The case of a trap-free system ($V = 0$, i.e., only a single Gaussian instead of two) has also been considered. In the calculations described below, $a = 1$ nm has been assumed.

The residence time of a carrier in a state i is defined using an exponential probability distribution [19]:

$$t_i = \frac{-\ln x}{\sum_{l \neq i} \nu_{il}}, \tag{6}$$

where x is a random number within the interval (0;1). The final state j is chosen using another random number according to the probability $p_{ij} = \nu_{ij} / \sum_{l \neq i} \nu_{il}$. Summarizing all the residence times, one obtains the transit time t_{tr} across the layer of the thickness $L = Na$ for this trial (i.e., for this run of a carrier across the sample). The morphology of a layer is changed before every trial to ensure statistical variation.

The MC simulations can serve as a reference for the MTR approach. The MTR model describes transport in thermal quasiequilibrium, and hence, the MC simulations need to reflect this. If charges are placed randomly in the DOS, an initial energetic relaxation process takes place, and quasiequilibrium conditions are established only at longer times. We take a shortcut to avoid the lengthy initial relaxation process and start by choosing the initial energy of a carrier directly from the distribution according to the quasiequilibrium function $g_{\text{occ}}(E) \propto g(E)\exp(-\frac{E}{kT})$ [15].

After having performed a rather large number of trials for a given set of parameters, the common way to calculate the drift mobility, which is proportional to the mean drift velocity of charge carriers, is as follows:

$$\mu = \frac{L}{F}\left\langle \frac{1}{t_{\text{tr}}} \right\rangle. \tag{7}$$

However, as shown in Fig. 3 for the case of a trap-free amorphous material and as detailed further for the M_0 and M_1 models in the Supplemental Material [18], we find that the drift mobility determined with Eq. (7) decreases considerably with the thickness of the layer increasing at least up

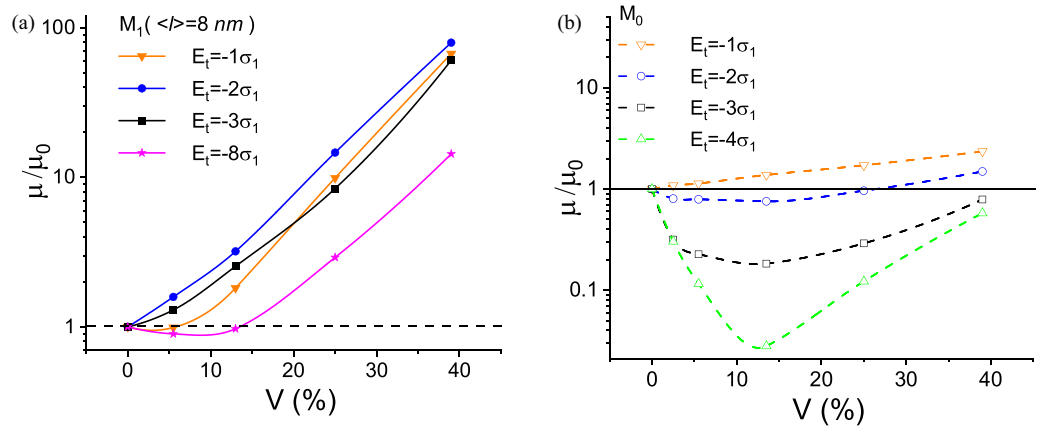

FIG. 4. The drift mobility, parametric in the mean energy depth of the lower Gaussian E_t. The other parameters: $T = 298$ K, $\langle l \rangle = 8$ nm, $eFa = kT$, $\sigma_1 = 50$ meV, $\sigma_2 = \sigma_1/3$; $2\gamma_2 a = 5$, and $2\gamma_1 a = 10$ for the hops involving and not involving crystallites, respectively. (a) Sample with crystallites, i.e., the M_1 model; (b) sample with traps, i.e., the M_0 model.

to $L = 100$ nm. This is unlikely to be the result of nonequilibrium transport because the initial energy distribution of charge carriers is premised to obey quasiequilibrium. The obvious reason is the neglect of charge-carrier diffusion in Eq. (7). If the field strength tends to zero, one obtains an apparent infinitely large mobility from Eq. (7) because the mean velocity $\langle L/t_{\rm tr} \rangle$ remains finite due to diffusion. This effect is important if a layer is rather thin and the electric field is not very strong, see Fig. 3(a).

To separate the effect of diffusion of charge carriers from the mobility, we apply the following correction. In addition to the averaged inverse transit times, driven by the electric field F, a diffusion-controlled value $\langle 1/t_{\rm tr}^0 \rangle$ is calculated for the case of the zero electric field ($F = 0$). Replacing the value $\langle 1/t_{\rm tr} \rangle$ by the corrected value $\langle 1/t_{\rm tr} \rangle - \langle 1/t_{\rm tr}^0 \rangle$ in Eq. (7), one obtains the corrected drift mobility, see Fig. 3. The corrected mobility is practically thickness independent and can be considered a characteristic parameter of a material if the disorder is rather small, see Figs. 3(a) and 3(b). The value of field strength $F = 2.57 \times 10^7$ V/m ($eFa/kT = 1$) chosen for basic calculations is a compromise. It is strong enough to provide an acceptable MC simulation time and reduce the effect of diffusion. On the other hand, the field is weak enough that the mobility does not significantly exceed the weak-field limit, as confirmed by calculations at a weaker field $eFa/kT = 0.4$.

A more general and computer time-saving way to obtain the bulk mobility (characteristic of the material, not the layer) is to extrapolate the thickness dependence of the apparent (i.e., not diffusion corrected) mobility, as outlined in Eq. (S1) and Fig. S3 in the Supplemental Material [18]. The previously obtained power-law thickness dependence for the apparent mobility [19] is reproduced. From test calculations using the example of a one-phase system (M_0 model) with $V = 0$, we show that both procedures correctly reproduce the well-known dependence of the mobility on temperature $\ln \mu = \text{const.} - C(\sigma_1/kT)^2$, $C \approx 0.44$, see Table S2 in the Supplemental Material [18]. In passing, we note that the method of MC calculations in this paper allows obtaining both the drift mobility in thin (<100 nm) layers and the actual drift mobility in the bulk based on calculations for only thin layers.

III. RESULTS

A key result of this paper is presented in Fig. 4. It shows plots of the bulk mobility as a function of the fraction of sites V that form the lower, narrower Gaussian DOS (G2). The bulk mobility was obtained by extrapolating the apparent mobility to large sample thickness as described in Supplemental Material [18]. The value of V denotes the fraction of G2 states, i.e., the fraction of states forming crystallites [for the case of the M_1 model, filled symbols, Fig. 4(a)], or the fraction of localized states from the lower Gaussian (for the case of the M_0 model, open symbols, Fig. 4(b). The mobility is normalized to its value at $V = 0$, i.e., the value for an amorphous material with a single-Gaussian DOS μ_0. The variable is the mean energy of the lower Gaussian E_t.

Figure 4(a) indicates that the mobility in the sample with crystallites typically exceeds the reference level μ_0 and increases with V almost exponentially. A shallow minimum near $V_* \cong 10\%$ is observed for large $|E_t|$. In contrast, in an amorphous material with localized trap sites with a trap energy of $|E_t| \geqslant 2\sigma_1$, the mobility first decreases with increasing V, passes through a deep minimum near $V_* \cong 10\%$, and then increases with V because charge carriers begin percolating among the traps. This is consistent with the literature. What is remarkable, however, is that the minimum of μ near V_* vanishes when the trap energy becomes comparable with the width of the DOS distribution of the G1 states. In this case, the mobility increases steadily with V and even exceeds the mobility of a trap-free system [Fig. 4(b)].

This observed increase in bulk mobility when shallow trap sites are introduced in an amorphous film is remarkable and deserves further analysis. To this end, we show in Fig. 5 how the mobility, normalized to the mobility of a trap-free system, changes as a function of the normalized trap depth $|E_t|/\sigma_1$, parametric in the trap concentration V. Figures 5(a) and 5(b) refer to simulations for 298 and 200 K, respectively. We observe that the maximum of μ/μ_0 increases with increasing trap concentration and shifts from slightly below $V_* \cong 10\%$ to slightly above $V_* \cong 10\%$ upon sample cooling from 298 to 200 K. The ratio of absolute mobilities at 200 and 298 K is $\mu_0(200)/\mu_0(298) \approx 0.5$. Considering that, in a

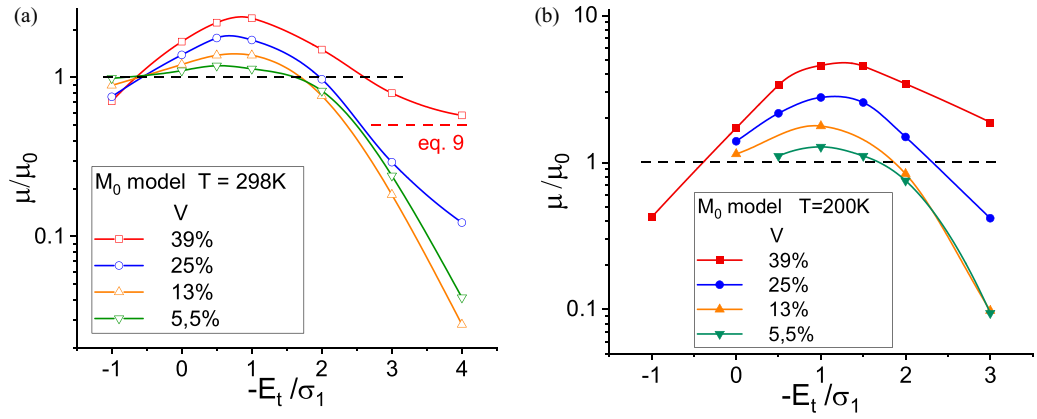

FIG. 5. Dependence of the bulk mobility in an amorphous material with trap sites (M_0 model) for two values of temperature on the average energy of the G2 states E_t and for various trap fractions V. The other parameters are the same as in Fig. 4. The horizontal black line shows the mobility value at $V = 0$. (a) Data for 298 K. The horizontal red line shows the analytic estimate for $E_t \to -\infty, V = 0.39$, according to Eq. (9) below. (b) Data for 200 K.

Gaussian-type DOS-distribution, on average, charge transport does not proceed among states close to the center of the DOS distribution but near a transport energy that is lower, we will further elaborate on this in the discussion section.

Similar regularities were also found for systems with crystallites, see Fig. 6, with the significant difference that $\mu/\mu_0 > 1$ in almost the entire considered range of parameters. Notably, the maximum of mobility can be two orders of magnitude higher than the mobility for the case of an amorphous material with a single-Gaussian DOS at room temperature. It is obvious that this must be due to the high hopping rate inside the crystallites and between crystallites due to presumed stronger delocalization of wave functions of G2 states and hence higher transfer rates.

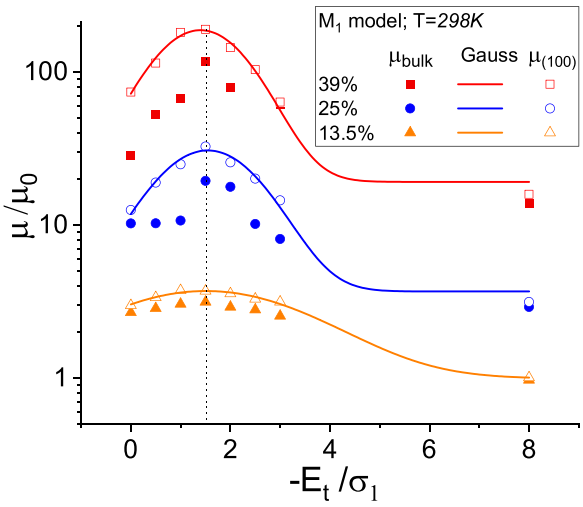

FIG. 6. Dependence of the mobility in a material with crystallites (M_1 model) on the mean energy of states in crystallites E_t. Here, $\mu_{(100)}$ is the mobility calculated for the sample thickness 100 nm, and μ_{bulk} is the mobility for the infinite sample. The data are shown for different values of the fraction of crystallites V for room temperature. The other parameters are the same as in Fig. 4.

The data in Fig. 6 pertain to drift mobility in a bulk system as well in a 100-nm film. The bulk mobility data are associated with considerable scatter, as we can see from Fig. 6, due to the extrapolation procedure. Figure 6 demonstrates that the qualitative dependence of the mobility on $|E_t|/\sigma_1$ is independent of the fraction of crystallites present V. The dependences of the drift mobility in the 100-nm film $\mu_{(100)}(E_t)$ can be well fitted by a combination of a Gaussian function and a constant, see the solid lines in Fig. 6. Data at 200 and 130 K, shown in the Supplemental Material [18], suggest that, analogous to the M_0 model shown in Fig. 5, the absolute value of the mean energy of G2 states at which mobility has a maximum $E_t^{\max}$ decreases with temperature.

The temperature dependence of the mobility is further studied in Fig. 7. It shows the temperature dependences of the drift mobility both at layer thickness $L = 100$ nm (small symbols, dashed lines) and for a bulk film (i.e., $L \to \infty$, large symbols, solid lines) in the material with crystallites (the M_1 model) for the fixed and rather large fraction of crystallites $V = 39\%$. The variable is the mean energy of states in crystalline phase E_t. For both the 100-nm film [Fig. 7(a)] and the bulk [Fig. 7(b)], the mobility decreases with temperature almost according to an Arrhenius law $\mu \propto \exp[-E_a/kT]$, with an activation energy corresponding to the σ_2 value of the G2 DOS distribution at $|E_t|/\sigma_1 > 3$, i.e., $E_a \approx 17$ meV, see Table S3 in the Supplemental Material [18] for details. An exception to this is the case of low trap depths ($|E_t|/\sigma_1 \leqslant 2$) in the bulk film. There, a faster decrease is observed, like the temperature-dependent decrease usually found in an amorphous material ($V = 0$), which has the form of $\mu \propto \exp\{-C(\sigma/kT)^2\}$ in Ref. [11], see curve 1 in Fig. 7.

IV. DISCUSSION AND COMPARISON WITH A MTR MODEL

The observations made for an amorphous system with singular traps [Figs. 4(b) and 5] can easily be understood at the qualitative level. First, for trap depths well exceeding σ_1, we see the classical signatures of percolative transport in trap systems that were studied extensively for molecularly doped

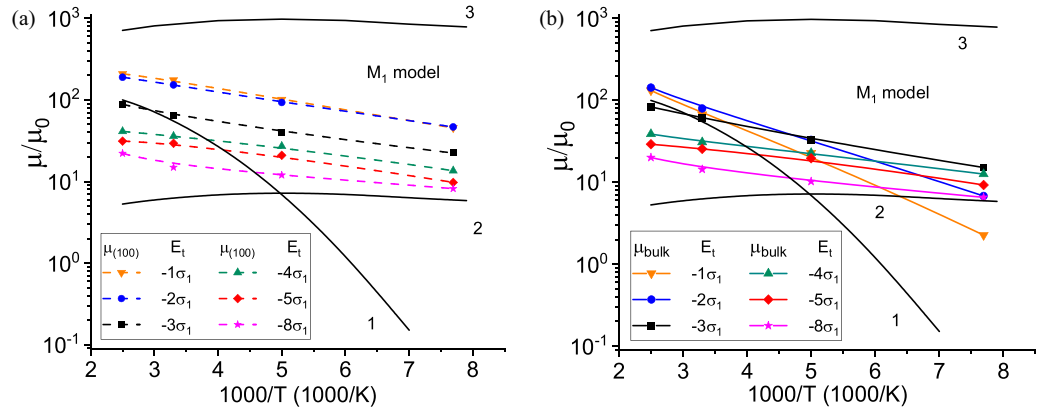

FIG. 7. Temperature dependences of the mobility in material of the M_1 model at various values of the mean energies of states in crystalline phase E_t; $V = 39\%$, for (a) a 100-nm film and (b) a bulk film. The solid black curves show analytic estimates from (1) the Gaussian disorder model (GDM) model ($V = 0$, $2\gamma a = 5$), (2) Eq. (16), and (3) Eq. (17), further below. The other parameters are the same as in Fig. 3. The mobility at $V = 0$ and $T = 298$ K, $2\gamma a = 10$ is denoted as μ_0.

polymers [20–24]. In brief, a small percentage of trap sites reduces mobility due to charge-carrier trapping and delayed thermal release. Once the percentage exceeds the amount needed for trap-to-trap transport (the percolation threshold V_*, typically ∼10%) the mobility increases again. Second, the interesting and perhaps less studied case is that of trap depth near σ_1, where we observe a mobility that exceeds that of the trap-free system. This mobility increase upon trapping is, at first sight, counterintuitive. It can, however, be understood when recalling that, in a Gaussian DOS, charge carriers are transported not in the center but at the transport energy E_C that is below the center, namely, $|E_c|/\sigma_1 = 0.87$ at room temperature [14]. Inserting trap sites at a depth of $|E_t|/\sigma_1 \approx 1$ thus increases the DOS that are very close to the transport level. In this way, transport is facilitated. We stress that transport occurs well within G1, as evident from Fig 5, in contrast to the percolative transport via deeper traps.

The level of complexity increases when the trap sites are not isolated but rather connected, as in the M_1 model, which considers oligomeric crystallites with increased coupling between each monomeric unit [Figs. 4(a), 6, and 7]. Like for isolated traps, we distinguish two cases, depending on trap depths. First, for very deep traps, e.g., $|E_t|/\sigma_1 \approx 8$, the transport shows the signature of percolative transport between the crystallites, with a percolation threshold of ∼10%. Below ∼10%, the mobility is reduced, albeit only marginally and only found for such very high trap depth, and the increase of mobility at high trap fractions such as 40% is about one order of magnitude [Fig. 4(a)]. Second, for moderate trap depth $|E_t|/\sigma_1 < 3$, a different transport regime prevails. The mobilities are higher than either the trap-free material or the materials with very deep traps and concomitant percolative transport in those traps (Fig. 6). This enhancement prevails even at low-crystallite concentrations and further increases with concentration. The fact that the mobility is not reduced even at, say, 5% of sites with a trap depth of $3\sigma_1$ is unexpected. The observation that the maximum of the mobility is reached for $|E_t|/\sigma_1 \approx 1.5$ provides a clue to the interpretation of this transport regime. We consider that transport is serial and occurs partially on the crystallites, with fast transport along the crystallites, and partially via the sites in G1 that are characterized by a weaker intersite coupling. Whether a particular jump occurs from a crystallite to another crystallite (G2 → G2) or to the amorphous sites (G2 → G1) will depend on the distance between crystallites and the energy of the adjacent amorphous sites and thus on whichever rate is faster. For these moderate trap depths $|E_t|/\sigma_1 < 3$, the transition from crystallite sites (G2) to amorphous sites (G1) is roughly isoenergetic, and transport occurs largely within the narrow distribution of the crystallite site energies. This results in an activation energy for transport approximately equal to σ_2 because percolative transport in G2 states prevails for $|E_t|/\sigma_1 > 3$ (Fig. 7).

For a quantitative description of transport in an amorphous material with localized trap sites (M_0 model), the MTR model provides a good starting point. This is illustrated in Fig. 8, which compares the data of Fig. 4(b) with the MTR model in its simple form, see Eq. (9) [10,12,14], and in the form

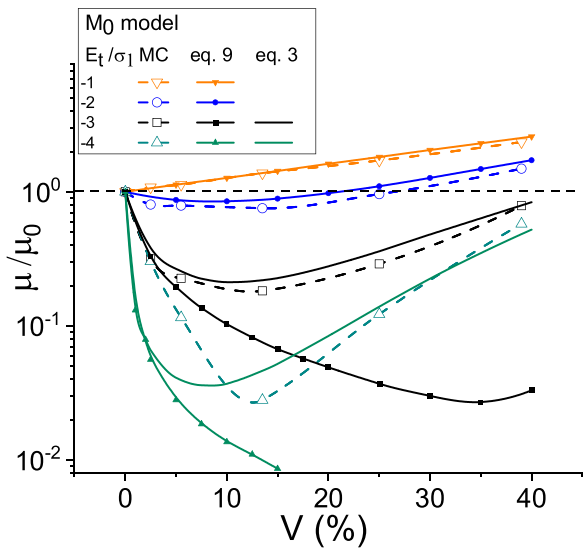

FIG. 8. Comparison of Monte Carlo (MC) results with analytic results of multiple trapping and release (MTR), see Eq. (9), and revised MTR, see Eq. (3), normalized to the mobility μ_0 of a trap-free amorphous material ($V = 0$).

advanced in this paper, see Eq. (3). In the simple form, the MTR model suggests that thermally activated jumps from very deep tail states to a transport level E_C control the mobility. The release rate is defined by Eq. (1) for this case. This means that, in Eq. (3), E_C is not a function but a constant (an effective transport level), and $E < E_C$; this is detailed further below. For a constant E_C, Eq. (3) reduces to

$$\mu \approx \frac{e\omega_0 a^2}{kT} \exp\left(-\frac{E_C}{kT}\right) \frac{\int_{-\infty}^{E_C} dE\, g(E)}{\int_{-\infty}^{E_C} dE\, g(E) \exp\left(-\frac{E}{kT}\right)}. \quad (8)$$

Using the DOS $g(E)$ from Eq. (4) in Eq. (8), one obtains

$$\mu = \mu_c \frac{\mathrm{erfc}\left(\varepsilon_c + \frac{1}{2\alpha_1}\right) + p\,\mathrm{erfc}\left[\frac{\sigma_1}{\sigma_2}(\varepsilon_c - \varepsilon_t) + \frac{1}{2\alpha_2}\right]}{2(1+p)}, \quad (9)$$

where $\mu_c = (e/kT)\nu_0 a^2 \exp(-2\gamma a)$, $\alpha_1 = kT/\sqrt{2}\sigma_1$, $\alpha_2 = kT/\sqrt{2}\sigma_2$, $\varepsilon_c = E_C/\sqrt{2}\sigma_1$, $\varepsilon_t = E_t/\sqrt{2}\sigma_1$, erfc is a complementary error function, and

$$p = \left(\frac{V}{1-V}\right) \exp\left[-\frac{\sigma_1^2 - \sigma_2^2}{2(kT)^2} - \frac{E_t}{kT}\right]. \quad (10)$$

Equation (9) gives the mobility that depends on the volume percentage of trap sites V through the parameter p. If the trap energy is near the transport energy, for example, for $|E_t|/\sigma_1 \approx 1$, then this simple variant of the MTR model agrees quantitatively with MC simulations for all volume fractions which is possible of trap sites, as evident from Fig. 8. For significantly lower trap energies, however, the simple MTR model [Eq. (9)] only reproduces the MC simulations for trap fractions well below the percolation threshold V_*. For a realistic case $p \gg 1$ (yet $V \ll 1$), which is possible if $E_t \ll -\sigma_1^2/kT$, Eq. (9) gives $\mu/\mu_0 \approx p^{-1} \approx (1/V)\exp[-\frac{|E_t|}{kT} + \frac{\sigma_1^2-\sigma_2^2}{2(kT)^2}]$, where $\mu_0 \equiv \mu(V=0)$, i.e., G2 states act as traps. If $V > V_*$, the concept of the transport level no longer works because thermal activation from the trap states (G2) to the states of the amorphous host (G1) becomes less likely than jumps between G2 states. In addition, jumps downward in energy (from G1 to G2 states) become more likely than thermal activation for some energy interval in the tail of G1 states, if the fraction V is rather large.

Thus, a generalized version of MTR formalism [15,17] is required, based upon Eq. (3). It accounts for the jumps downward in energy. The difficulty in deriving an analytical expression for the bulk mobility lies in the fact that $E_C(E)$ is a function of E, i.e., not a constant. To derive an expression for $E_C(E)$, we follow the approach of Refs. [14–16]. One can calculate the mean release rate of a carrier from a state with energy E from the condition $n(\omega, E) = B$ with the percolation factor $B \approx 2.77$ [25]; $n(\omega, E)$ is the mean number of target neighbor sites whose hopping rates are not smaller than a given value of ω, i.e., $\nu(E, E', r) \geqslant \omega \equiv \nu_0 \exp(-u)$. The latter condition means that $r \leqslant r_*(E, E', u) = (2\gamma)^{-1}[u - \frac{E'-E}{kT}\eta(E'-E)]$, see Eq. (5); $\eta(E'-E)$ is a step function. One obtains the equation for the release rate $\omega \equiv \nu_0 \exp(-u)$ by integrating the DOS function in (r, E') space:

$$n[u(\omega), E] = \mathrm{B} = \frac{4\pi}{3} \int_{-\infty}^{E+kTu} dE' g(E') r_*^3(E, E', u). \quad (11)$$

The upper limit of integration is defined from the equation $r_* = 0$. Introducing the parameter $E_{\mathrm{tr}} \equiv E + kTu$, i.e., expressing the mean release rate as $\omega = \nu_0 \exp[-(E_{\mathrm{tr}} - E)/kT] \equiv \omega_0 \exp[-(E_C - E)/kT]$, $\omega_0 \equiv \nu_0 \exp(-2\gamma a)$, one obtains from Eq. (11)

$$\frac{\pi}{6(\gamma kT)^3}\left[(E_{\mathrm{tr}} - E)^3 \int_{-\infty}^{E} g(E')dE' + \int_{E}^{E_{\mathrm{tr}}} g(E')(E_{\mathrm{tr}} - E')^3 dE'\right] = B, \quad E_{\mathrm{tr}} = E_C + 2\gamma akT. \quad (12)$$

Equation (12) defines implicitly the function $E_C(E)$, i.e., not a constant. In this way, Eq. (3) with $E_C(E)$ as defined through Eq. (12) represents the generalized version of the MTR formalism presented in this paper. The mobility is a function of the trap fraction V via the function $g(E)$, see Eq. (4). As is evident from Fig. 8, Eq. (3) with $E_C(E)$ from Eq. (12) gives a satisfying agreement with the MC simulations for all trap fractions and all trap depths considered, although for very deep traps, the minimum of the mobility is found at lower G2 site content V than in the MC simulations.

In the case of $E \to -\infty$, the dependence on the energy in the expression in Eq. (12) vanishes because the first term, describing jumps downward in energy, is negligible. Hence, the function $E_C(E)$ approaches a constant value, i.e., to an effective transport level E_{C} [14], which results from the equations:

$$\frac{\pi}{6(\gamma kT)^3} \int_{-\infty}^{E_{\mathrm{tr}}} g(E')(E_{\mathrm{tr}} - E')^3 dE' = B, \quad E_{\mathrm{tr}} \equiv E_C + 2\gamma akT. \quad (13)$$

This is what is used for the simple MTR model [Eq. (9)].

In case of very deep G2 states, $E_t \to -\infty$, and $V > V_*$ jumps occur only between G2 states. Since these states are located randomly in space and $\sigma_2 < kT$ at room temperature, one can estimate the mobility from the r-percolation result [20]. Assuming isoenergetic trap states, one obtains

$$\mu(E_t \to -\infty) \approx \frac{e\nu_0}{kT}(0.87a)^2\, V^{-2/3} \exp(-1.74\gamma a V^{-1/3}), \quad (14)$$

where $aV^{-1/3}$ is the mean distance between trap states. The result of Eq. (14) for $V = 0.39$ and $T = 298$ K is shown by the horizontal red line in Fig. 5(a). The agreement with the MC simulation is satisfying.

When the trap sites form extended crystallites (M_1 model) and have a high fraction V, transport cannot be meaningful described by a particular transport energy E_C for the matrix material G1. Instead, it is useful to analyze the dependence of the average energy of occupied states E_{av} as a function of E_t. At thermal quasiequilibrium, we can use $g_{\mathrm{occ}}(E) = g(E)\exp(E/kT)$ with $g(E)$ from Eq. (4) and obtain

$$E_{\mathrm{av}} = \frac{\int_{-\infty}^{\infty} dE E g_{\mathrm{occ}}(E)}{\int_{-\infty}^{\infty} dE\, g_{\mathrm{occ}}(E)} = \frac{-\frac{\sigma_1^2}{kT} + p\left(E_t - \frac{\sigma_2^2}{kT}\right)}{1+p}, \quad (15)$$

with p defined by Eq. (10). The relation between E_{av} and E_t is shown in Fig. 9.

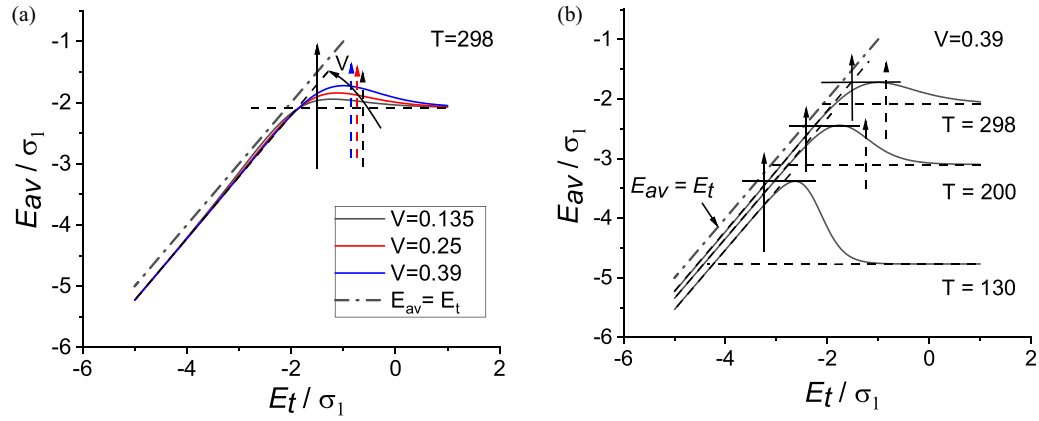

FIG. 9. Dependences of the average energy, as calculated from Eq. (15), on the fraction of G2-states, V (a) and temperature (b). Solid and dashed vertical arrows show the values of E_t at which the maximum mobility is achieved in material with crystallites (M_1 model, value taken from Fig. 6) or with singular traps (M_0 model, value taken from Fig. 5), respectively. The dashed-dotted diagonal line indicates the values for $E_{av} = E_t$. Here, σ_1 is 50 meV. The horizontal dashed lines denote to the average equilibrium energies of occupied G1 states $-\sigma_1^2/kT$.

When G2 is well below or above the center of G1 distribution describing the amorphous matrix, then the average energy of occupied states corresponds simply to the equilibrium energy of the lowest-energy distribution, i.e., $E_{av}(E_t) = E_t - \sigma_2^2/kT$ if G2 distribution is well below the center of G1 states and $E_{av}(E_t) = -\sigma_1^2/kT$ otherwise. In the former case, the energy E_{av} increases with increasing of E_t. When E_t is above the average equilibrium energy of G1 states $-\sigma_1^2/kT$, then the occupied G2 states raise the average energy of the entire ensemble above the value of $-\sigma_1^2/kT$. This is even more the case for large volume fractions of G2, as illustrated in Fig. 9(a). The occupation probability of G2 states decreases with increasing their energy; hence, the energy E_{av} decreases with increasing of E_t. In this way, the maximum in the dependences $E_{av}(E_t)$ in Fig. 9 is formed.

Like in the case of singular traps (M_0), for extended crystalline traps (M_1), the mobility also goes through the maximum as a function of the trap depths, see Fig. 6. This maximum of the mobility occurs near the maximum of the average energy E_{av}^{max}, as indicated in Fig. 9 by the vertical arrows.

If the G2 states are very deep and their fraction V is not small, only these states participate in transport. We recall that hops within a crystallite of G2 states are much faster than any other hops; hence, the rate-limiting step is (practically) nonactivated but long-distance hops between crystallites. As the G2 states become shallower, hops from G2 to G1 states become faster because the activation energies of jumps decrease; hence, these hops begin to make a significant contribution to transport, thus leading to an increase in mobility. Once $E_t \gg E_{av}^{max}$, thermal activation from G1 to G2 states slows down transport; hence, the mobility decreases with an increase of E_t. Eventually, G2 states become empty, and transport is completely controlled by G1 states (amorphous phase). Thus, mobility has a maximum if $E_t \approx E_{av}^{max}$ since G1 states can effectively act as bridges between crystallites.

The mobility increases with V, see Fig. 4, and has a weak temperature dependence at $E_t \ll -\sigma_1$ due to small energy disorder of G2 states ($\sigma_2 < kT$). Due to this circumstance and due to the increased jump frequency of G2-G2 jumps relative to G1-G1 jumps, the mobility at $V = 0.39$ exceeds the mobility at $V = 0$ and room temperature, i.e., $\mu/\mu_0 > 1$, even at the lowest considered temperature, see Fig. 7. One may estimate a lower limit for the temperature-dependent carrier mobility at $V = 0.39$ by considering very deep traps, where the rate-limiting long-distance jumps between crystallites dominate. In this case,

$$\mu(E_t \to -\infty) \approx \frac{e\nu_0}{kT} a_*^2 \exp\left[-2\gamma_2 ra - 0.44\left(\frac{\sigma_2}{kT}\right)^2\right], \quad (16)$$

in which the mean distance between centers of crystallites $a_* = \langle l \rangle V^{-1/3}$. Equation (16) yields curve 2 in Fig. 7, using $r = 2 + 0.87 = 2.87$, where $2a$ is the minimal hopping distance between crystallites in the numerical model and 0.87 arises from the r-percolation theory [25]. At lower temperatures, σ_2 controls the temperature dependence as expected, whereas at higher temperatures, the assumption of an infinitely low E_t causes the $1/kT$ prefactor to dominate. A higher limit for the temperature-dependent carrier mobility is given if transport occurs only over crystallite sites, i.e., if $V = 1$, with

$$\mu_{max} = \left(\frac{e\nu_0 a^2}{kT}\right) \exp\left[-2\gamma_2 a - 0.44\left(\frac{\sigma_2}{kT}\right)^2\right]. \quad (17)$$

Finally, we comment on the observed difference in temperature-dependent mobility between thin ($L = 100$ nm) films and thick films with $L \to \infty$. Figure 7(b) shows that the MC simulations indicate a steeper temperature dependence for shallow traps ($E_t > -3\sigma_1$) in the thick film than the thin film. We consider that, for larger layer thicknesses, less probable jumps from G2 to states deep in the tail of G1, followed by slow thermally activated release, can be realized, and this reduces the bulk mobility rapidly with decreasing temperature, in contrast to the case of thin films.

V. CONCLUSIONS

This paper is a theoretical study on the mobility of charge carriers in a thin layer of a two-phase disordered organic material employing kinetic MC simulation and analytic theory. The model is designed to mimic a system in which

crystallites, characterized by low static disorder ($\sigma_2 < kT$) and enhanced electronic coupling, are embedded in a more disordered (amorphous) phase with a standard deviation of the DOS distribution $\sigma_1 = 3\sigma_2$. The mobility of charge carriers has been studied as a function of the volume fraction V of the crystalline phase, the energetic offset between the centers of the distributions of the amorphous phase and the crystallites (E_t), and on temperature. For comparison, also the mobility in a layer of an amorphous material containing localized trapping sites with a double Gaussian energy distribution has been considered.

We find that, in a system with isolated traps, the mobility features a minimum near $V = 10\%$ and increases afterwards because then charge carriers begin percolating among the traps. This is a well-documented phenomenon, tractable by the MTR formalism [15]. The unexpected observation is that this mobility minimum is absent, and μ increases continuously with increasing V if the trap depth is close to the standard deviation σ_1 of the DOS distribution of the amorphous phase. The reason is that then the narrow trap distribution of G2 states overlaps with the transport energy E_C, and concomitantly, the number of sites that control charge transport is increased. When the traps are replaced by crystallites, the mobility features a very shallow minimum near $V = 10\%$ yet only if the energetic offset between both phase is high (e.g., $|E_t|/\sigma_1 = 8$). Otherwise, μ increases continuously with increasing V by up to two orders of magnitude relative to the mobility of the neat amorphous phase and features a pronounced maximum at $|E_t|/\sigma_1 \approx 1.5$, independent of V. For $|E_t|/\sigma_1 \geqslant 3$, the temperature dependence of μ becomes independent of E_t. The temperature dependence is Arrhenius-like with activation energies of 20–30 meV. These results can be rationalized in terms of a superposition of two different transport modes, namely, (i) percolative transport among the crystallites when the energetic offset between parent phase and the crystallites is large ($|E_t|/\sigma_1 > 3$) and (ii) hopping transport at a transport level that is formed by the overlap between the crystallite sites and sites of the parent phase ($|E_t|/\sigma_1 < 3$). The great increase of the mobility upon blending the amorphous phase by crystallites is due the fact that the crystallites are conductive elements.

In a recent analytic work, Emin [26] also considers the conductivity in a two-phase system with particular attention on the dependence on the carrier concentration yet neither on the concentration of the crystallites nor on temperature. He also disregards the role of energetic disorder, known to be crucial for understanding the properties of a real-world organic semiconductors. In this paper, we demonstrate that the explicit consideration of disorder is crucial for rationalizing the dependence of the charge-carrier mobility in a two-phase organic system as a function of the concentration of crystallites and of their energetic depth.

From the viewpoint of applications, the result of this paper allows rationalizing charge transport in organic systems that are prone to aggregation. A timely example is a film of Y6 that acts as electron acceptor in organic solar cells [27]. Absorption spectra of Y6 films [28] show that, at room temperature, a Y6 film is a mixture of an amorphous phase and crystalline domains. The absorption spectrum of the amorphous component is broad, while that of the crystallites is narrow and redshifted relative to that of the amorphous phase. Interestingly, the electron mobility in a PM6:Y6 solar cell is 8×10^{-4} cm^2/Vs [27] which is a comparatively high value for a disordered organic film. Experimentally, the calculated results could be best verified by the charge extraction (of injected carriers) by linearly increasing voltage in the metal-insulator-semiconductor structures (MIS-CELIV) method, providing rather small injection current during the interval of negative bias. In this case, it is possible to measure mobility at low concentration of carriers in quasiequilibrium. Hence, in summary, in this paper, we offer guidelines of optimizing composition and energy offset between the components in an amorphous material with either crystallites or isolated trap states embedded in it.

ACKNOWLEDGMENTS

A.Yu.S. and V.R.N. acknowledge support of the Russian Science Foundation, Project No. 22-22-00612. A.K. and H.B. thank the Volkswagen Foundation (the project "Understanding the dependence of charge transport on morphology in organic semiconductor films") for support.

[1] R. J. Kline, M. D. McGehee, E. N. Kudnikova, J. Liu, and J. M. J. Frechet, Adv. Mater. **15**, 1519 (2003).
[2] A. Zen, J. Pflaum, S. Hirschmann, W. Zhuang, F. Jaiser, U. Asawapirom, J. P. Rabe, U. Scher, and D. Neher, Adv. Funct. Mater. **14**, 757 (2004).
[3] P. Pingel, A. Zen, R. D. Abellon, F. C. Grozema, L. D. A. Siebbeles, and D. Neher, Adv. Funct. Mater. **20**, 2286 (2010).
[4] H. H. Choi, A. F. Paterson, M. A. Fusella, J. Panidi, O. Solomeshch, N. Tessler, M. Heeney, K. Cho, T. D. Anthopoulos, B. P. Rand *et al.*, Adv. Funct. Mater. **30**, 1903617 (2020).
[5] W. L. Kalb, S. Haas, C. Krellner, T. Mathis, and B. Batlogg, Phys. Rev. B **81**, 155315 (2010).
[6] F. Steiner, C. Poelking, D. Niedzialek, D. Andrienko, and J. Nelson, Phys. Chem. Chem. Phys. **19**, 10854 (2017).
[7] I. Vladimirov, M. Kühn, T. Geßner, F. May, and R. T. Weitz, Sci. Rep. **8**, 14868 (2018).
[8] M.-A. Muth, G. Gupta, A. Wicklein, M. Carrasco-Orozco, T. Thurn-Albrecht, and M. Thelakkat, J. Phys. Chem. C **118**, 92 (2014).
[9] T. Meier, H. Bässler, and A. Köhler, Adv. Optical Mater. 2100115 (2021).
[10] V. I. Arkhipov, P. Heremans, E. V. Emelianova, G. J. Adriaenssens, and H. Bässler, J. of Non-Crystalline Solids **299–302**, 1047 (2002).
[11] H. Bässler, Phys. Stat. Sol. B **175**, 15 (1993).
[12] V. I. Arkhipov, E. V. Emelianova, and G. J. Adriaenssens, Phys. Rev. B. **64**, 125125 (2001).
[13] A. I. Rudenko and V. I. Arkhipov, Phil. Mag. B **45**, 177 (1982).

[14] V. R. Nikitenko and M. N. Strikhanov, J. Appl. Phys. **115**, 073704 (2014).
[15] R. Saxena, V. R. Nikitenko, I. I. Fishchuk, Ya. V. Burdakov, Yu. V. Metel, J. Genoe, H. Bässler, A. Köhler, and A. Kadashchuk, Phys. Rev.B **103**, 165202 (2021).
[16] M. D. Khan, V. R. Nikitenko, and O. V. Prezhdo, J. Phys. Chem C **125**, 20230 (2021).
[17] F. W. Schmidlin, Phys. Rev. B **16**, 2362 (1977).
[18] See Supplemental Material at https://link.aps.org/supplemental/10.1103/PhysRevB.108.085301 for the parameters of the numerical model and dependence of the drift mobility on the layer thickness, mean energy of crystallites, and temperature.
[19] A. Ya. Freidzon, A. A. Bagaturyants, Ya. V. Burdakov, V. R. Nikitenko, and V. A. Postnikov, J. Phys. Chem C **125**, 13002 (2021).
[20] D. M. Pai, J. F. Yanus, and M. Stolka, J. Phys. Chem **88**, 4714 (1984).
[21] I. I. Fishchuk, A. K. Kadashchuk, A. Vakhnin, Yu. Korosko, H. Bässler, B. Souharce, and U. Scherf, Phys. Rev. B **73**, 115210 (2006).
[22] R. Coehoorn and P. A. Bobbert, Phys. Status Solidi A **209**, 2354 (2012).
[23] J. Cottaar, R. Coehoorn, and P. A. Bobbert, Phys. Rev. B **82**, 205203 (2010).
[24] Y. Y. Yimer, P. A. Bobbert, and R. Coehoorn, J. Phys.: Condens. Matter **20**, 335204 (2008).
[25] S. D. Baranovskii, Phys. Status Solidi A **215**, 1700676 (2018).
[26] D. Emin, Phil. Mag. **99**, 1225 (2019).
[27] L. Perdigón-Toro, L. Q. Phuong, F. Eller, G. Freychet, E. Saglamkaya, J. I. Khan, Q. Wei, S. Zeiske, D. Kroh, S. Wedler *et al.*, Adv. Energy Mater. **12**, 2103422 (2022).
[28] D. Kroh, F. Eller, K. Schötz, S. Wedler, L. Perdigón-Toro, G. Freychet, Q. Wei, M. Dörr, D. Jones, Y. Zou *et al.*, Adv. Funct. Mater. **32**, 2205711 (2022).